

DOI 10.24425/ae.2024.150886

Time-harmonic finite element model for brushless doubly-fed induction machine in natural operating mode

MARIUSZ JAGIEŁA , MARIAN ŁUKANISZYN

*Opole University of Technology
Faculty of Electrical Engineering, Automatic Control and Informatics
45-758 Opole, ul. Prószkowska 76
e-mail: [✉ m.jagiela/m.lukaniszyn@po.edu.pl](mailto:mailto:m.jagiela/m.lukaniszyn@po.edu.pl)*

(Received: 24.11.2023, revised: 22.08.2024)

Abstract: The natural mode of operation for the brushless doubly-fed induction machine is a particular instance of synchronism at a so-called natural rotor velocity when one stator winding is powered by an AC and the other by a DC voltage source. Consequently, in addition to the rotating magnetic field, there exists a magnetic field that is fixed to the stator frame of reference. Analysis in this specific mode is essential as the natural velocity arises from the choice of pole numbers, thereby determining machine efficiency. However, this presents a significant challenge when it comes to mathematical modeling using complex-valued steady-state models through either equivalent-circuit or finite element analysis. This paper presents a study on the extension of the recently-proposed steady-state complex-valued finite element model for the brushless doubly-fed induction machine to enable its application in the natural operating mode. A high correlation with the data obtained from a time-stepping model is obtained for the extended model when subjected to both low and high levels of saturation of the magnetic circuit. This extension makes the whole approach applicable in all operating conditions and modes of the brushless doubly-fed induction machine. Considering the nearly two orders of magnitude lower computational costs associated with analysis via the proposed model compared to time-stepping analysis, it is particularly useful in scenarios that involve extensive computations and require multiple cases to be considered such as design sensitivity analysis, topology optimization or a connection with machine learning techniques.

Key words: doubly-fed machines, finite elements, induction machines, mathematical modelling, steady state, synchronous machines



© 2024. The Author(s). This is an open-access article distributed under the terms of the Creative Commons Attribution-NonCommercial-NoDerivatives License (CC BY-NC-ND 4.0, <https://creativecommons.org/licenses/by-nc-nd/4.0/>), which permits use, distribution, and reproduction in any medium, provided that the Article is properly cited, the use is non-commercial, and no modifications or adaptations are made.

1. Introduction

The brushless doubly-fed induction machine (BDFIM) is a synchronous induction machine that presents numerous advantages for future wind-power generation systems. These benefits include low maintenance requirements due to a brushless structure, the absence of permanent magnets, voltage-fault ride-through capability, and the ability to control velocity, torque, and reactive power using fractional power [1–4]. Despite these merits, its commercialization has yet to occur primarily due to control issues [5–8]. The latter will materialize as a consequence of the ongoing refinement and enhancement of mathematical models. Various methodologies have been used for the BDFIM of a whole hierarchy of models utilized in AC machines, encompassing single-phase equivalent-circuit models [9–13], coupled-circuit models [14], magnetic equivalent circuit-based models [15], and finite element (FE) models [16–18]. This study primarily concentrates on the latter ones. The finite element analysis for the BDFIM is normally performed in the time domain, requiring costly manipulation of waveform quantities rather than just magnitudes. However, the latter can be achieved by utilizing the FE model described in [18], which incorporates the complex magnetic vector potential. The proposed approach decreases computational time by a factor of 1/60 when compared to the transient time-domain model. Also, it maintains good accuracy across a wide range of BDFIM operating conditions and modes, with the exception being the natural mode where it is not applicable in its current form. The importance of the natural mode stems from the correlation between machine efficiency and its natural velocity, given that BDFIM operating velocity is within a range of $\pm 30\%$ deviation from its natural velocity [1, 13]. It thus becomes important to be able to investigate the BDFIM operation at this particular point. To this moment this has been done using steady-state equivalent-circuit model [12]. However, this type of model proves efficient solely upon experimental identification of their parameters. The proposed field model in [18] has the ability to rapidly determine BDFIM characteristics and does not require experimental identification. Therefore, the objective of this study is to extend the proposed model by presenting a consistent theory, implementing it in a computer program and validating the accuracy of the extended time-harmonic finite element model for a BDFIM in natural mode.

2. Features of BDFM in natural model

Each BDFIM is designed to continuously operate powered through two stator windings (each connected to AC voltage sources) with carefully selected pole-pair numbers $-p_p$ and p_c . The rotor winding cross-couples electromagnetically the stator windings through a particular nested-loop structure with $p_p + p_c$ poles [1–6]. The angular frequency of the current in the rotor winding induced by the fundamental harmonic components of the air-gap magnetic field of ordinal numbers p_p and p_c (with respectively, positive and negative phase sequences), fulfils the relationship [1, 3, 9]

$$\underbrace{\omega_p - p_p \Omega_r}_{\substack{\text{frequency of rotor winding current} \\ \text{induced by stator winding space} \\ \text{harmonic } p_p \text{ of positive phase sequence}}} = \underbrace{-(\omega_c - p_c \Omega_r)}_{\substack{\text{frequency of rotor winding current} \\ \text{induced by stator winding space} \\ \text{harmonic } p_c \text{ of negative phase sequence}}} \quad (1)$$

By introducing rotor slips, s_p with respect to the stator winding with the p_p pole number, and s_c , with respect to the stator winding with the p_c pole number, the above formula can also be written in the equivalent form:

$$\omega_p s_p = -\omega_c s_c. \tag{2}$$

From (1) it can be deduced that the synchronous velocity of the rotor is

$$\Omega_r = \frac{\omega_p + \omega_c}{p_p + p_c}. \tag{3}$$

Assume that the stator winding with the pole number p_p is the power winding, whilst the one with the pole number p_c is the control winding. Typically, the BDFIM is utilized in a manner where the winding p_p is connected to the grid, thereby establishing a fixed frequency. Subsequently, the winding p_c receives power from a converter with adjustable voltage and frequency. A particular scenario arises whilst a demand for velocity compels the control voltage frequency to assume a value of 0 hertz. This operating state is commonly referred to as the natural mode [12], as it occurs at a particular value of synchronous velocity called the natural velocity.

$$\Omega_n = \frac{\omega_p}{p_p + p_c}. \tag{4}$$

In this scenario, the operation of the BDFIM is akin to that of a conventional synchronous machine due to AC and DC voltage supplies used, albeit with more intricate performance characteristics and control mechanisms. Furthermore, the DC supply is actually a three-phase voltage with zero frequency and a negative phase sequence. In the natural mode, all functionalities of the BDFIM operating in a double-feed mode remain intact except for the unidirectional power flow via the control winding as depicted in Figs. 1(a) and 1(b). The diagrams depicted in Figs. 1(c) and 1(d) illustrate that the electromagnetic coupling of the control winding in natural mode solely occurs unidirectionally, specifically through the current of the power which results in magnetomotive force (mmf) induced in the rotor winding. Conversely, it is important to note that while this process occurs, no back electromotive force (emf) is generated in the control winding from the rotor flux. The presented depictions of electromagnetic interactions lead to the necessary evolution of the standard steady-state equivalent-circuit model for the BDFIM [9] (see Fig. 1(e), shown in Fig. 1(f)). The time-harmonic finite element model presented in [18] is also subject to evolution within this context. The bridge between the equivalent circuit and the actual finite element model is that the lumped parameters of the former can be conveniently extracted from the latter, although we aim to address this topic in our future work. The control of machine torque and VARs flow in natural mode can be achieved by adjusting the absolute value and phase angle φ of a control voltage. The vector \mathbf{V}_c that represents the voltage in three phases at the terminals of the control winding in Fig. 1(d) is described by the formula

$$\mathbf{V}_c = \text{Re} \{ \underline{\mathbf{V}}_c \} = \text{Re} \left\{ V_{DC} \begin{bmatrix} 1 \\ e^{-j4\pi/3} \\ e^{-j2\pi/3} \end{bmatrix} \right\}, \tag{5}$$

where: V_{DC} is the DC voltage supplying the converter as shown in Fig. 1(a), j represents the imaginary unit, and Re denotes the real component.

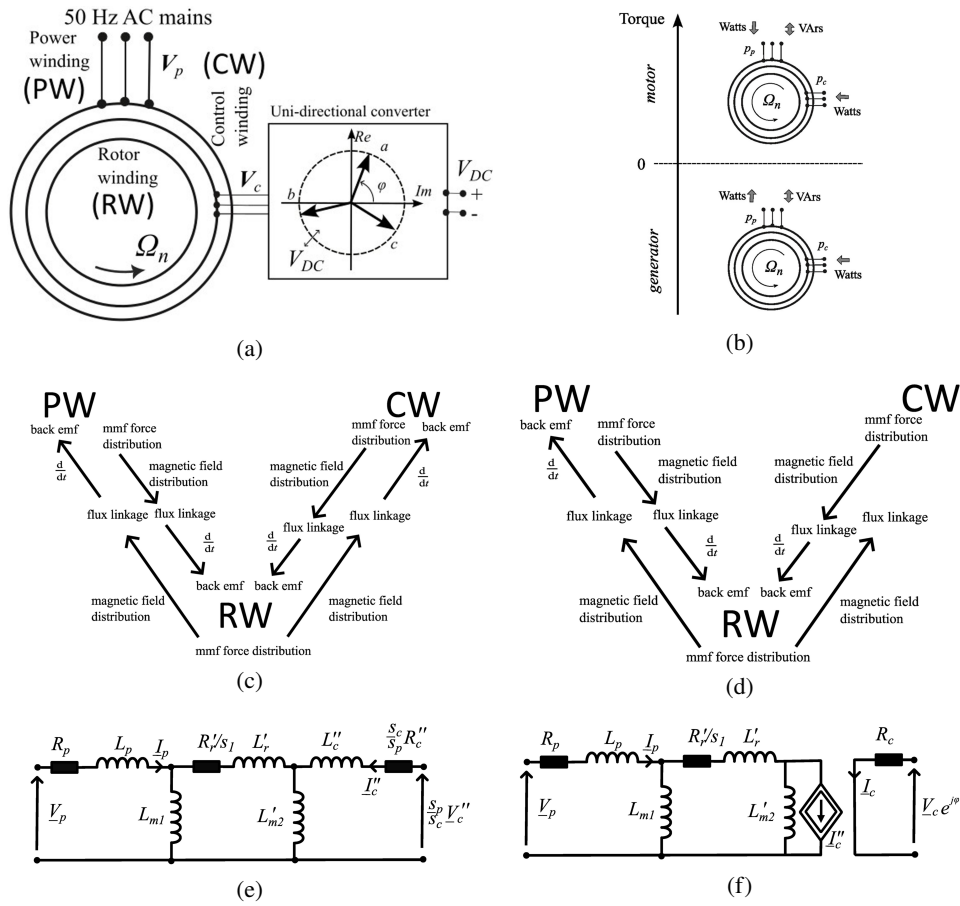


Fig. 1. BDFIM in natural mode: (a) driving principle; (b) active and reactive power flows for motoring and generating operations; (c), (d) logical flowchart diagrams illustrating, respectively the electromagnetic cross-coupling in BDFIM in all except natural modes and in natural mode; (e), (f) single-phase equivalent circuit models, respectively in all except natural modes and in natural mode, in natural mode

As noticed, this particular situation can be considered an operating point of the BDFIM in the double-feed mode. If the BDFIM is required to operate continuously in natural mode, one benefit is that a simpler converter structure can be used, compared to supplying from two AC sources. Table 1 outlines the crucial functional characteristics of a BDFIM operating in natural mode.

R_p and L_p are the power winding resistance and leakage inductance, R_c'' and L_c'' are the control winding resistance and leakage inductance referred to the power winding side, L_{m1} is the magnetizing inductance of the power winding, L'_{m2} is the magnetizing inductance of the control winding, R_r and L_r are the rotor winding resistance and inductance referred to the power winding side, R_c'' is the control winding resistance referred to the power winding side, V_p is the power winding voltage, V_c'' is the control winding voltage referred to the power winding side, φ is the phase angle of the control winding voltage.

Table 1. Basic characteristics of BDFIM operating in natural mode

Rotor slip	$s_n = \frac{p_c}{p_p + p_c}$
Rotor velocity relative to velocity of rotating magnetic field	$\frac{\Omega_n}{\omega_p} = \frac{p_p}{p_p + p_c}$
Efficiency	low due to high s_n
Speed control	possible by varying the frequency of power winding voltage, but impractical as it requires utilization of two converters for both power and control winding sides
Torque control	by varying $ V_{DC} $ and φ using uni-directional fractionally rated converter
Control of VARs	by varying $ V_{DC} $ and φ using uni-directional fractionally rated converter
Possible practical application	constant-velocity grid-tied power generation standalone power generation constant-velocity-variable-power geared drive

In an open-access work [18] we developed a new frequency-domain finite element model for the steady-state analysis of the BDFIM operating in simple induction, and single- and double-feed synchronous modes considering non-linearity of the magnetic materials. In the concluding section of the former study, we arrived at a sound verdict that the detailed model fails to depict the BDFIM in natural mode. This conclusion was based on two following factors.

i) The mathematical formulation of the model hinges upon integrating two slips, namely s_p and s_c . In natural mode, the latter tends towards infinity.

ii) The magnetic flux density distribution within the stator of a BDFIM operating in natural mode is comprised of both time-varying rotating and stator-frame-fixed components. To effectively address the modeling of magnetic non-linearity using the effective permeability concept for sinusoidal fields, further justification and testing must be applied to the current method developed thus far.

Later on, it will become apparent that the equations derived in [18] require a minor modification to accommodate for the natural mode.

3. Mathematical foundation for steady-state operation of BDFIM in natural mode

3.1. Generic equations of magnetic field

In the analysis of induction machines, it is common to substitute the real-valued magnetic vector potential with its complex counterpart [18–20]. The 2-nd distribution of the fundamental time component of a rotating magnetic field in such a case can be represented by the complex

magnetic vector potential \underline{A} . A generic form of this substitution can be written as

$$A(r, \theta, t) = \operatorname{Re} \left\{ \underline{A}(r, \theta) e^{j(\omega t - p\theta)} \right\}, \quad (6)$$

where: (r, θ, t) are the spatial coordinates and time, p is the number of pole-pairs and ω is the angular frequency. The Ampere law for the time-harmonic magnetic field in the BDFIM can be expressed in the form

$$-\operatorname{div} \frac{1}{\mu} \mathbf{grad}(A) = J - \sigma \left(\frac{dA}{dt} - \frac{U}{l} \right), \quad (7)$$

where: μ and σ are, respectively, the magnetic permeability and conductivity, J is the current density due to the current source, U is the voltage across the rotor bar, and l is the machine's active length. Using the rotor frame of reference, in natural mode the distributions of magnetic fields due to the power winding driven from the AC source and due to the control winding driven from the DC source can, respectively, be written in the forms:

$$A_p(r, \theta, t) = \operatorname{Re} \left\{ \underline{A}_p(r, \theta) e^{j\omega_p s_n t} \right\}, \quad (8)$$

$$A_c(r, \theta, t) = \operatorname{Re} \left\{ \underline{A}_c(r, \theta) e^{j p_c \Omega_n t} \right\}. \quad (9)$$

From (1) it can be deduced that $p_c \Omega_n = \omega_p s_n$. After simple manipulations it can be shown that the magnetic field can be expressed as a combination of magnetic vector potentials A_p and A_c as their angular frequencies are the same. This new quantity will be referred to as $A' = A_p + A_c$ [18]. It is evident that Eq. (7) undergoes modification accordingly.

$$-\operatorname{div} \frac{1}{\mu'} \mathbf{grad}(\underline{A}') = -\sigma \left(j s_n \omega_p \underline{A}' - \frac{U'}{l} \right), \quad (10)$$

where U' is the sum of complex voltages across rotor bars due to fields A_p and A_c , and $\mu' \equiv \mu (|\mathbf{curl} \underline{A}'|)$. In the BDFIM, stator Eqs. (8) and (9) take different forms, namely

$$A_p(r, \theta, t) = \operatorname{Re} \left\{ \underline{A}_p(r, \theta) e^{j\omega_p t} \right\}, \quad (11)$$

$$A_c(r, \theta, t) = \operatorname{Re} \left\{ \underline{A}_c(r, \theta) e^{j\omega_c t} \right\} = \operatorname{Re} \left\{ \underline{A}_c(r, \theta) \right\}. \quad (12)$$

The complex magnetic vector potential $\underline{A}' = \underline{A}_p + \underline{A}_c$ can, however, be used globally given that:

i) no direct electromagnetic coupling exists between the harmonic components of magnetic flux density between the stator windings due to the sensible selection of pole-pair numbers p_p and p_c [1, 9];

ii) the quantity \underline{A}_c is a complex number coupling with real and imaginary parts of \underline{A}' (despite formally the DC drive of the control winding) because the voltage drive \underline{V}_c is the complex number and so are currents and magnetomotive force of the control winding.

Summing up, Eq. (7) for the region of the stator results in two separate complex equations, each describing the magnetic system attributed to the corresponding winding.

$$-\operatorname{div} \frac{1}{\mu} \mathbf{grad} \left(\underline{A}_p \right) = \underline{J}_p, \quad (13)$$

$$-\operatorname{div} \frac{1}{\mu} \mathbf{grad} (\underline{A}_c) = \underline{J}_c. \quad (14)$$

As stated in i)-ii), it becomes evident that this problem can be solved using a single global magnetic vector potential $\underline{A}' = \underline{A}_p + \underline{A}_c$ and a single equation in the form:

$$-\operatorname{div} \frac{1}{\mu'} \mathbf{grad} (\underline{A}') = \underline{J}', \quad (15)$$

where $\underline{J}' = \underline{J}_p + \underline{J}_c$ is the sum of complex current densities due to, respectively, the power control winding, and μ' is expressed in exactly the same way as for the region of the rotor.

Equations (10) and (15) are to be built considering the ones describing electric circuits formed by the stator and rotor windings. The system of field-circuit equations describing the BDFIM in all except the natural modes was described in detail in [18]. As noticed, in natural mode the magnetic couplings of the BDFIM are different in terms of decoupling the control winding (see Fig. 2). In the field-circuit model, this is reflected by the modification of only a circuit equation describing the current of the control winding, which takes a much simpler form than in [18].

$$\underline{V}_c = \mathbf{R}_c \underline{I}_c, \quad (16)$$

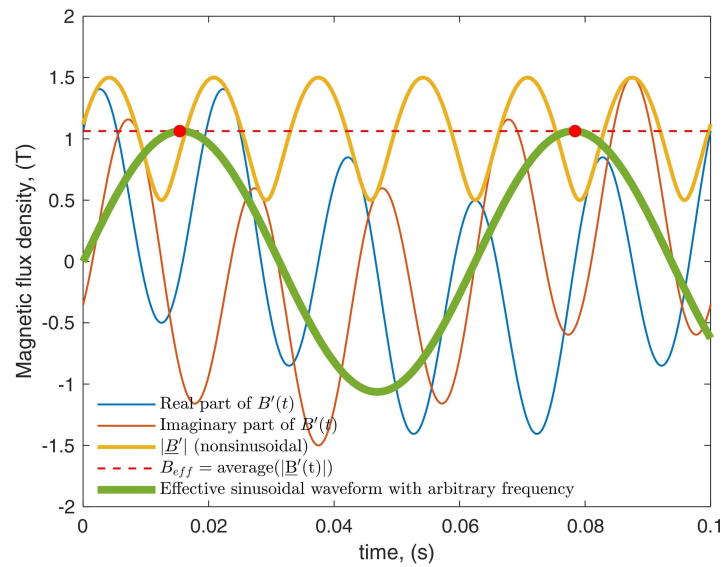
where \mathbf{R}_c is the matrix containing the resistances of the control winding and \underline{I}_c is the vector of phase currents. The remaining equations require no alteration. For the natural mode, the whole system of equations receives the following final form:

$$\begin{bmatrix} S(\mu') + js_n \omega_p \mathbf{R} & -\mathbf{W}_p & -\mathbf{W}_c & \mathbf{D}_r \ell^{-1} & \mathbf{0} \\ j\omega_p \mathbf{W}_p^T & \mathbf{R}_p + j\mathbf{X}_p & \mathbf{0} & \mathbf{0} & \mathbf{0} \\ \mathbf{0} & \mathbf{0} & \mathbf{R}_c & \mathbf{0} & \mathbf{0} \\ -js_n \omega_p \mathbf{D}_r^T & \mathbf{0} & \mathbf{0} & \mathbf{G}_r & \mathbf{K} \\ \mathbf{0} & \mathbf{0} & \mathbf{0} & \mathbf{K}^T & \mathbf{R}_r \end{bmatrix} \begin{bmatrix} \underline{\phi} \\ \underline{I}_p \\ \underline{I}_c \\ \underline{U} \\ \underline{I}_r \end{bmatrix} = \begin{bmatrix} \mathbf{0} \\ \underline{V}_p \\ \underline{V}_c \\ \mathbf{0} \\ \mathbf{0} \end{bmatrix} e^{j\varphi}, \quad (17)$$

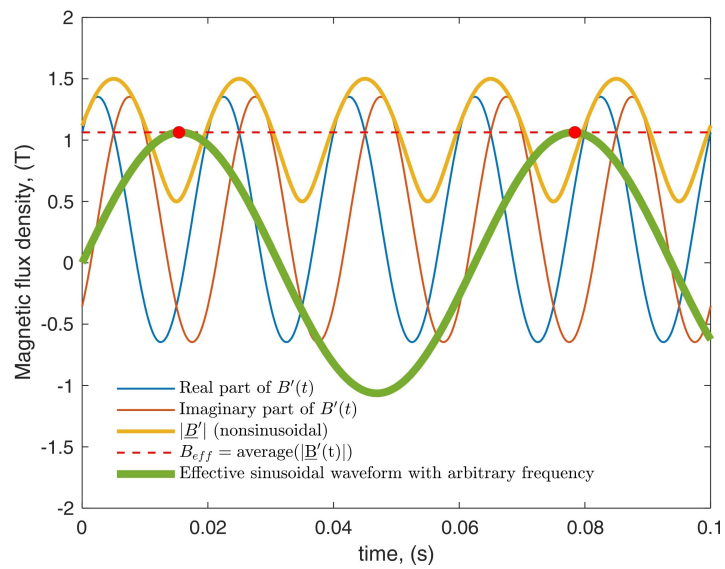
where: $S(\mu')$ and \mathbf{R} are the distributed reluctance and conductance matrices, respectively, \mathbf{W}_p and \mathbf{W}_c are the stator winding distribution matrices of the power and control winding, respectively, \mathbf{D}_r is the rotor winding distribution matrix, \mathbf{R}_p and \mathbf{X}_p are the power winding resistance and end-winding reactance matrix of the power winding, respectively, \mathbf{G}_r is the lumped rotor bar conductance matrix, \mathbf{K} is the auxiliary coupling matrix and \mathbf{R}_r is the rotor end-connections resistance matrix. The $\underline{\phi}$ vector comprises values representing magnitudes of the magnetic vector potential \underline{A}' , the \underline{I}_p vector comprises the magnitudes of power winding currents, the \underline{U} vector comprises the magnitudes of voltages across the rotor bars, and the \underline{I}_r vector comprises the magnitudes of currents of the rotor winding.

System (17) enables the determination of all machine characteristics in relation to rotor velocity (slip s_p). By manipulating the angle φ , one can alter the variations of the characteristics in relation to the synchronous angle at a given velocity. In this context, the computations utilizing the described time-harmonic model are nearly as simple as employing the equivalent circuit model. The electromagnetic torque of the BDFIM is calculated using the Maxwell stress tensor formula

$$T_e = \frac{\ell r_a^2}{2\pi\mu_0} \operatorname{Re} \left\{ \oint_C B'_r B'_\theta^* d\theta \right\}, \quad (18)$$



(a)



(b)

Fig. 2. Time variations of real value, imaginary value and modulus of magnetic flux density \underline{B}' for a hypothetical case of double-feed for $|B_p| = 1$ T, $|B_c| = 0.5$ T: (a) $\omega_p = 100\pi$ rad/s, $\omega_c = 10$ Hz; (b) natural mode $\omega_p 100\pi$ rad/s, $\omega_c = 0$ Hz

where r_a is the average air-gap radius, μ_0 is the vacuum permeability, B'_r and B'_θ are the radial and circumferential components of magnetic flux density determined by applying the **curl** operator to the magnetic vector potential \underline{A}' , and C is the integration path in the BDFIM air-gap.

3.2. Modeling non-linearity of magnetic materials for zero hertz at the control winding terminals

All modeling techniques for traditional induction machines, in which the non-linearity of steel cannot be disregarded, rely on the notion of effective permeability that is contingent solely upon the magnitude of the magnetic field quantity [19, 20]. In a BDFIM, the time-varying magnetic field displays modulated wave characteristics that cannot be captured by a single magnitude. In [18] we introduced a workaround founded on the expansion of established induction machine methodologies. Our hypothesis was that a sinusoidal waveform, which accurately reflects the modulated waveform in terms of effective saturation level, exists. We analysed the modulated waveform of the magnetic flux density (radial or circumferential component) as a combination of two complex single-harmonic waveforms with different frequencies. It can be demonstrated that the modulus of this complex sum varies over time and its variation is non-linear and non-harmonic concerning magnitudes of the component waveforms. Nevertheless, it has been demonstrated that the time-averaged modulus serves as an effective determinant of the saturation level of magnetic materials. In natural mode, wherein one waveform possesses zero frequency, the summation of component fields in the stator must be regarded in the following way:

$$\underline{B}'(t) = \underline{B}_p e^{j\omega_p t} + \underline{B}_c e^{j(\omega_c=0)t} = \underline{B}_p e^{j\omega_p t} + \underline{B}_c, \quad (19)$$

where \underline{B}_p and \underline{B}_c are the local values of magnetic flux density due to the power and control winding, respectively, that are determined by performing a spatial decomposition of the magnetic field distribution \underline{A}' into harmonic components with pole numbers p_p and p_c as shown in [18]. The waveform in the rotor consists of the two time-varying components

$$\underline{B}'(t) = \underline{B}_p e^{j\omega_p s_n t} + \underline{B}_c e^{j p_c \Omega_n t}. \quad (20)$$

In both regions of analysis, the effective permeability is determined from the following Formula [20]

$$\mu(B_{\text{eff}}) = \left(\frac{4}{\pi} \int_0^{\pi/2} \frac{\sin^2 \alpha}{\mu(B_{\text{eff}} \sin \alpha)} d\alpha \right)^{-1}, \quad (21)$$

where $B_{\text{eff}} = \text{average}(|\underline{B}'(t)|)$ and α is the auxiliary independent variable.

It may come as a surprise that the effective permeability model remains practically unchanged for both non-zero and zero frequency in driving the control winding. However, a more insightful analysis of the variations resulting from Formula (19) clearly exposes such a possibility. This is done in Fig. 2 that compares the variations of $\underline{B}'(t)$ and $|\underline{B}'(t)|$ for the two different scenarios. It can be deduced that B_{eff} has the same value in Figs. 2(a) and 2(b). This results from the mathematical features of the waveform $|\underline{B}'(t)|$, namely when only one of the component waveforms has non-zero frequency, like Formula (19), the frequency (either zero or non-zero) of the other component waveform has an impact only on the shape of $|\underline{B}'(t)|$; however, it does not exert an influence on its

mean value. This observation validates the consistency of the developed methodology, which in practice can be applied to any feasible operating conditions of the BDFIM.

4. Implementation and validation of non-linear time-harmonic model

The authors employed a MATLAB language program to execute the elaborated model, as there was an absence of commercially accessible FE software environments with the ability to amalgamate the derived equations. The graphical representation of the data flow utilized by the computer program employed to calculate BDFIM characteristics is depicted in Fig. 3. In order to validate the approach through numerical means, an identical model was implemented utilizing a time-domain moving-rotor-mesh finite element technique. To ensure geometrical consistency between both models, they are created from the same finite element mesh. The specifications of the BDFIM are given in Table 2, while its geometry and core material magnetisation characteristics are comprehensively delineated in [18, 21].

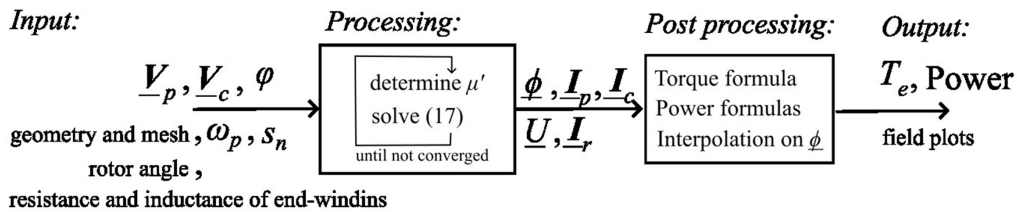
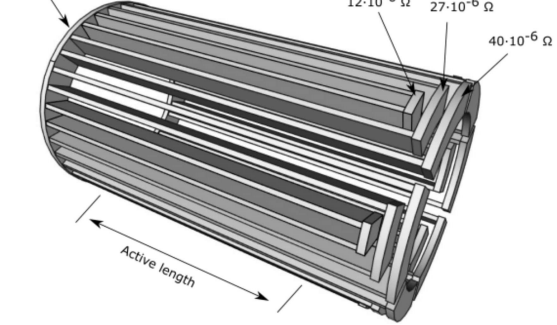
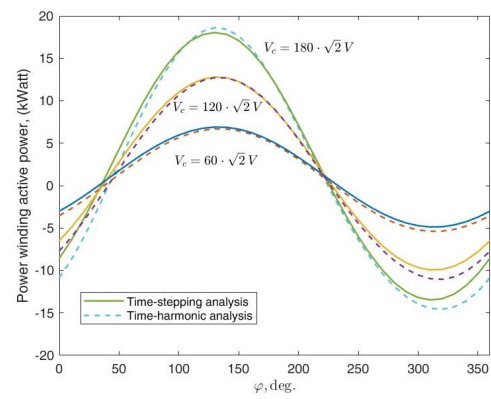
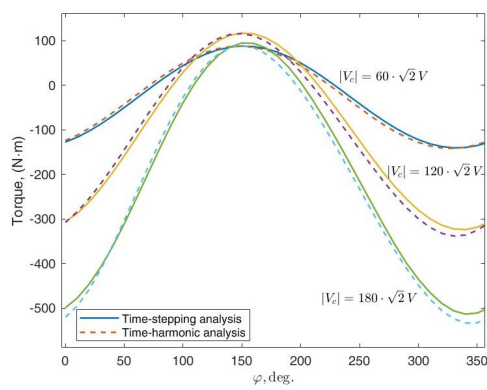


Fig. 3. Data flow in the developed computer program

Figure 4 displays the results of a comparison of torque variations, rms currents, and power in-take through the power winding at three distinct voltage levels supplied as control winding input. The quantities are determined and graphed as a function of the angle φ . For each value of control voltage and φ , a time-stepping analysis is conducted over five periods of the power winding voltage to obtain the steady state. The three distinct levels of the control winding voltage correspond to varying degrees of core saturation: small, medium, and heavy. Although the results obtained at the highest level of control voltage are beyond the feasible practical values, they do demonstrate that the proposed time-harmonic model performs well even under a heavily saturated magnetic circuit. The complex torque variation shown in Fig. 4(a) around $\varphi = 150^\circ$ – which initially decreases before increasing with increasing control voltage – is due to an interplay between synchronous and asynchronous components rather than magnetic circuit saturation itself. As shown in [9], at a constant velocity, the torque of the BDFIM can be described by the parabola $T = c_2 V_{r2}^2 + c_1 V_{r2} + c_3$, where $c_1 - c_3$ are factors dependent on the machine parameters and operating conditions and V_{r2} is a voltage across the reactance $\omega_p L_{m2}'$ (see Figs. 1(e)– (f)). As evidenced by the results, the model performs accurately under a range of operating conditions, including those that are extreme. Its demonstrated precision is such that it would be deemed acceptable by virtually any design methodology.

Table 2. Basic specifications of tested BDFIM

Active length	124 mm
Power winding	pole-pair number $p_p = 2$, two-layer, phase resistance = 2.3Ω , end-winding leakage inductance = 0.65 mH , 10 turns per coil
Control winding	pole-pair number $p_c = 4$, two-layer, phase resistance = 5.4Ω , end-winding leakage inductance = 1.0 mH , 20 turns per coil
Rotor winding	material – copper End-ring sector, resistance $12 \cdot 10^{-6}\ \Omega$ End-loop resistance $12 \cdot 10^{-6}\ \Omega$ $27 \cdot 10^{-6}\ \Omega$ $40 \cdot 10^{-6}\ \Omega$ 



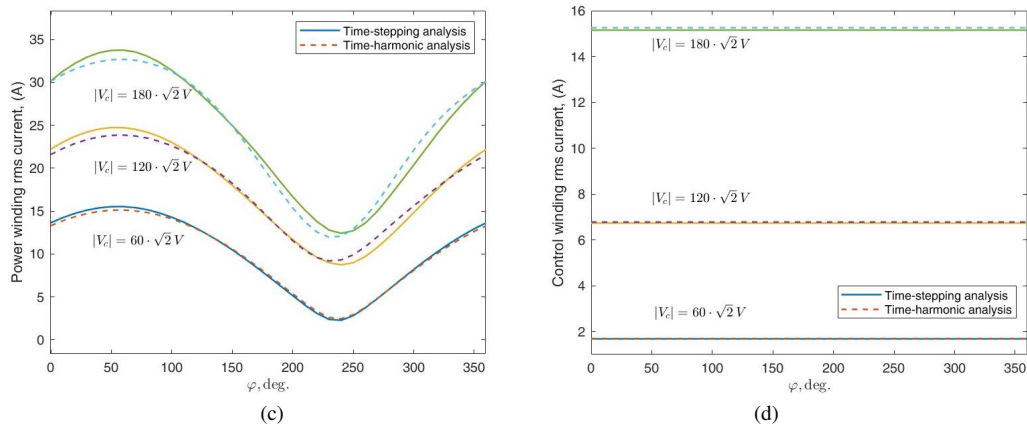
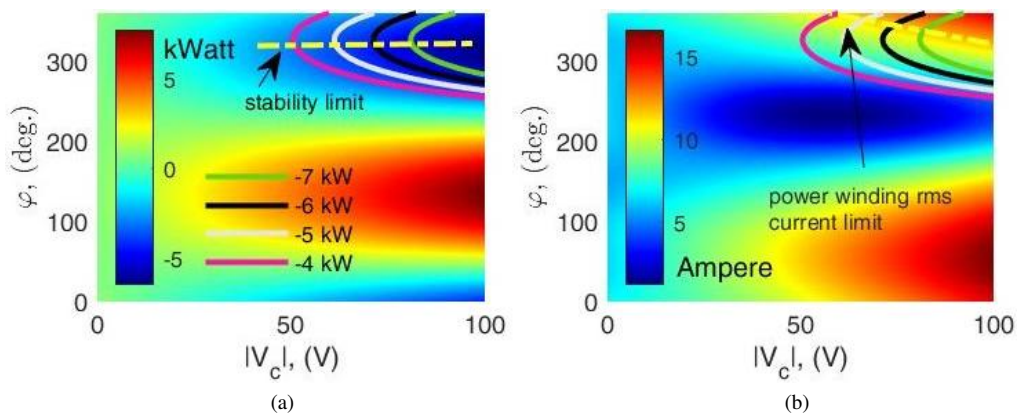


Fig. 4. Results of computations for $V_p = 230\sqrt{2} \text{ V}$, $\omega_p = 100\pi \text{ rad/s}$: (a) electromagnetic torque; (b) intake of active power by power winding; (c) power winding rms current; (d) control winding rms current. Positive torque is for motoring operation, negative torque is for generating operation. Positive power values mean watts delivered to machine, negative power watts injected to the source

5. Conclusions

The aim of this paper is to employ a recently developed method for steady-state modeling of the BDFIM using a 2-nd time-harmonic finite element model encompassing its entire practical operating velocity range, even during conditions where one stator voltage frequency is set to zero hertz. Specifically, it has been demonstrated that extrapolation of the proposed effective magnetic permeability model can be executed in such a case. As a consequence, the methodology has attained a comprehensive applicability across all operational scenarios. The computational efficiency of the proposed model is approximately (1/60)-th that of a time-stepping model. Depending on the saturation level, a single problem is solved within 30–60 seconds. This renders it not only suitable for determining individual characteristics but also for performance maps, as depicted in Fig. 5.



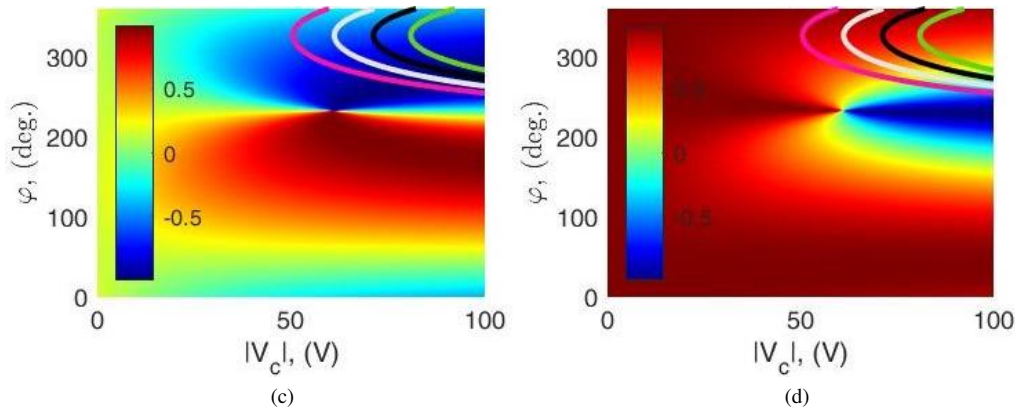


Fig. 5. Performance maps of BDFIM in natural mode considering feasible range of control winding voltage. Thick contour lines in each sub-figure delineate a few selected paths of constant power at generating operation. The demarcated loci can be utilized to deduce the V-curves analogous to ones of conventional synchronous machine: (a) mechanical power; (b) rms phase current of control winding; (c) cosine of power angle of power winding; (d) sine of power angle of power winding. Positive power values mean power delivered to machine, negative power mean power injected to the grid

The low computational costs associated with the proposed model hold potential for performing design sensitivity analysis or topology optimisation and/ or the connection with machine learning techniques among other possible applications.

Moreover, the overall concept can be extended to a three-dimensional space, which has yet to be used for BDFIMs. In particular, when utilizing the BDFIM in future applications involving high power output, it may be essential to employ these models to analyse the distribution of stray losses occurring in both the stator and rotor core end regions. Performing such an analysis through three-dimensional time-stepping models currently lacks practical benefits due to the significant amount of time involved.

References

- [1] McMahon R.A., Roberts P., Wang X., Tavner P.J., *Performance of BDFM as generator and motor*, IET Electr. Power Appl., vol. 153, no. 2, pp. 289–299 (2006), DOI: [10.1049/ip-epa:20050289](https://doi.org/10.1049/ip-epa:20050289).
- [2] Han P., Cheng M., Ademi S., Jovanovic M.G., *Brushless doubly-fed machines: opportunities and challenges*, Chin. Journ. of Electr. Eng., vol. 4, no. 2, pp. 1–17 (2018).
- [3] Strous T.D., Polinder H., Ferreira J.A., *Brushless doubly fed induction machines for wind turbines: developments and research challenges*, IET Electric Power Applications, vol. 11, no. 6, pp. 991–1000 (2017).
- [4] McMahon R., Tavner P., Abdi E., Malliband P., Barker D., *Characterising brushless doubly fed machine rotors*, IET Electric Power App., vol. 7, no. 7, pp. 535–543 (2013), DOI: [10.1049/iet-epa.2012.0238](https://doi.org/10.1049/iet-epa.2012.0238).
- [5] Ademi S., Jovanovic M., *High-efficiency control of brushless doubly-fed machines for wind turbines and pump drives*, Energy Conversion and Management, vol. 81, no. 1, pp. 120–132 (2014), DOI: [10.1016/j.enconman.2014.01.015](https://doi.org/10.1016/j.enconman.2014.01.015).

- [6] Tohidi S., *Analysis and simplified modeling of brushless doubly-fed induction machine in synchronous mode of operation*, IET Electric Power Applications, vol. 10, no. 2, pp. 110–116 (2016), DOI: [10.1049/iet-epa.2015.0217](https://doi.org/10.1049/iet-epa.2015.0217).
- [7] Su J., Chen Y., Zhang D., Kang Y., *Stand-Alone brushless doubly fed generation control system with feedforward parameters identification*, IEEE Trans. Ind. Informatics, vol. 11, no. 15, pp. 6011–6022 (2019).
- [8] Oraee A., Abdi E., McMahan R.A., *Converter rating optimisation for a brushless doubly fed induction generator*, IET Renewable Power Generation, no. 9, pp. 360–367 (2015), DOI: [10.1049/iet-rpg.2014.0249](https://doi.org/10.1049/iet-rpg.2014.0249).
- [9] Roberts P.C., McMahan R., Tavner P.J., Maciejowski J.M., Flack T.J., *Equivalent circuit for the brushless doubly fed machine (BDFM) including parameter estimation and experimental verification*, IET Electric Power Appl., vol. 152, no. 4, pp. 933–942 (2005), DOI: [10.1049/ip-epa:20045106](https://doi.org/10.1049/ip-epa:20045106).
- [10] Ramtin S., Madani S.M., Lipo T.A., Agha Kashkooli M.R., Ataei M., Ademi S., *Voltage-Dip Analysis of Brushless Doubly Fed Induction Generator Using Reduced T-model*, IEEE Trans. Industr. Electronics, vol. 66, no. 10, pp. 7510–7519 (2018), DOI: [10.1109/TIE.2018.2880713](https://doi.org/10.1109/TIE.2018.2880713).
- [11] Yu K., Tag P., *Novel Equivalent Circuit Model and Theoretical Analysis of Doubly Fed Machine*, IEEE Trans. Energy Conv., vol. 34, no. 2, pp. 1073–1081 (2018).
- [12] Ge J., Xu W., Liu Y., Xiong F., *Novel Equivalent Circuit Model Applicable to All Operation Modes for Brushless Doubly Fed Induction Machines*, IEEE Trans. Industr. Electronics, vol. 69, no. 12, pp. 12540–12550 (2022), DOI: [10.1109/TIE.2022.3144567](https://doi.org/10.1109/TIE.2022.3144567).
- [13] Oraee A., McMahan R., Abdi E., Abdi S., Ademi S., *Influence of Pole-pair Combinations on the Characteristics of the Brushless Doubly Fed Induction Generator*, IEEE Trans. Energy Conv., vol. 35, no. 3, pp. 1151–1159 (2020), DOI: [10.1109/TEC.2020.2982515](https://doi.org/10.1109/TEC.2020.2982515).
- [14] Olubamiwa O.I., Gule N., Kamper M.J., *Coupled circuit analysis of the brushless doubly fed machine using the winding function theory*, IET Electr. Power Appl., vol. 14, no. 9, pp. 1558–1569 (2020).
- [15] Gorginpour H., Oraee H., McMahan R.A., *A novel modeling approach for design studies of brushless doubly fed induction generator based on magnetic equivalent circuit*, IEEE Trans. Energy Conv., vol. 28, no. 4, pp. 902–912 (2013).
- [16] Wang X., Strous T.D., Lahaye D., Polinder H., Ferreira J.A., *Finite element modeling of brushless doubly-fed induction machine based on magneto-static simulation*, Proc. of IEMDC, Coeur d'Alene, ID, USA, pp. 315–321 (2015), DOI: [10.1109/IEMDC.2015.7409077](https://doi.org/10.1109/IEMDC.2015.7409077).
- [17] Wang X., Strous T.D., Lahaye D., Polinder H., Ferreira J.A., *Modeling and Optimization of Brushless Doubly-Fed Induction Machines Using Computationally Efficient Finite-Element Analysis*, IEEE Trans. Ind. Appl., vol. 52, no. 6, pp. 4525–4534 (2016), DOI: [10.1109/TIA.2016.2593715](https://doi.org/10.1109/TIA.2016.2593715).
- [18] Jagiela M., Wang X., McMahan R., Garbiec T., *Time-harmonic field-circuit model for brushless doubly fed induction machine*, IET Electric Power Applications, Wiley, pp. 965–975 (2023), DOI: [10.1049/elp2.12317](https://doi.org/10.1049/elp2.12317).
- [19] Bastos J.P.A., Sadowski N., *Electromagnetic Modelling by Finite Element Methods*, Marcel-Dekker, New York (2003).
- [20] Takorabet N., Laporte B., Mezani S., *An approach to compute saturated induction motors in steady state*, Proc. of IEMDC, USA, Madison, vol. 2, pp. 1646–1650, 1210672 (2003), DOI: [10.1109/IEMDC](https://doi.org/10.1109/IEMDC).
- [21] Jagiela M., *2D-Dxf File with Geometry Description for D270 BDFIM Stator and Rotor Cores* (2022).